Published in final edited form as:
Bioconjug Chem. 2008 September ; 19(9): 1880–1887. doi:10.1021/bc800160b.

Shape effects of nanoparticles conjugated with cell-penetrating peptides (HIV Tat PTD) on CHO cell uptake

Ke Zhang[†,‡], **Huafeng Fang**[†], **Zhiyun Chen**[†], **John-Stephen A. Taylor**[†], and **Karen L. Wooley**[†,‡]

Department of Chemistry, Washington University School of Arts & Sciences, 1 Brookings Drive, Saint Louis, Missouri 63130 and Department of Radiology, Washington University School of Medicine, 510 South Kingshighway Boulevard, Saint Louis, Missouri 63110

Abstract

In order to probe the nanoparticle shape/size effect on cellular uptake, a spherical and two cylindrical nanoparticles, whose lengths were distinctively varied, were constructed by the selective crosslinking of amphiphilic block copolymer micelles. Herein, we demonstrate that, when the nanoparticles were functionalized with the protein transduction domain of human immunodeficiency virus type 1 Tat protein (HIV Tat PTD), the smaller, spherical nanoparticles had a higher rate of cell entry into Chinese Hamster Ovary (CHO) cells than did the larger, cylindrical nanoparticles. It was also found that nanoparticles were released after internalization, and that the rate of cell exit was dependent on both the nanoparticle shape and the amount of surface-bound PTD.

INTRODUCTION

The plasma membrane of a cell serves as one of the major barriers against inward transportation of extraneous materials, such as a gene and/or a nanoscale synthetic delivery system. Modern synthetic designs have incorporated various cell-penetrating peptides (CPPs), borrowed initially from virus particles, to facilitate their uptake by cells through a receptor-independent pathway (1), whose mechanism is not yet completely understood. The ability of a nanostructure to translocate across the cell plasma membrane is of fundamental and practical interest, and will determine the possible outcomes of the nanomaterial in a biological context. Nanostructures of various sizes, shapes and chemical compositions have gained access to the cell's interior with or without the assistance of CPPs, including metal nanoparticles (2), dendrimers (3), liposomes (4), single-walled carbon nanotubes (5), and virus-mimics (6), etc. However, the amount of assistance provided by the CPPs for the nanoparticles to be internalized by a cell may be limited (7); eventually the influence of the size and geometric features of the cargo will become increasingly important. Recently, Chan *et al* (2,8) probed the effects of size and shape, for penetratin-coated gold nanoparticles within the 10−100 nm range, on the endo- and exocytosis by mammalian cells. A non-linear relationship between size and uptake was found, and 50 nm spherical particles were identified as having the highest cell uptake. On the micrometer scale, Mitragotri *et al* investigated the shape effect by synthesizing a variety of geometrically-anisotropic polystyrene particles, whose phagocytosis rates were found to be strongly dependent on the shape of the microparticle (9). However, a study to compare across the 10−1000 nm region using particles of similar chemical nature is still unavailable. The mechanism of CPP-assisted cell internalization of the cylindrical structure (several μm in length), which was recently discovered to enhance *in vivo* circulation times much beyond that

[†]Department of Chemistry
[‡]Department of Radiology

which can be achieved by other morphologies (10), remains largely unknown. It is, therefore, of interest to bridge the gap between nanoscale and microscale structures, in terms of comparing and understanding their CPP-assisted cell uptake and release.

Advances in the design and synthesis of well-controlled block copolymers have given rise to the rapid growth of a new class of complex nanostructures having various compositions, morphologies, sizes, and physical and biological properties (11-13), which can serve as the primary materials for examination of the effects of nano- to microstructure size and shape on cell internalization. For example, shell-crosslinked assemblies of amphiphilic block copolymers have in recent years attracted researchers to explore their biological and medicinal uses (14-17). These shell-crosslinked nanoparticles have enhanced stability compared to micelles and are capable of carrying biologically-active molecules, which drastically change the biological behavior of the nanoparticles (15,18). In this work, we take advantage of the vast array of morphologies available to polymer micelle-based nanoparticles (19-23) and their ability to allow for chemical modifications (24,25) in order to study the shape and size effects of a nanoscopic particle in a cellular system.

Herein, we report a method to create spherical and cylindrical nanostructures, of different lengths, from self assembly of block copolymers. After functionalizing the nanostructures with the protein transduction domain of human immunodeficiency virus type 1 Tat protein (HIV Tat PTD, one commonly used CPP, having the sequence: GYGRKKRRQRRR), we demonstrate that the smaller spherical particles (on the 10 nm scale) are internalized by CHO cells faster than are the larger cylindrical particles (20 or 30 nm diameters and larger than 200 nm in one dimension). It is also shown that, upon cellular uptake, the spherical particles are released from the cell, and the rate of release is also dependent on the amount of PTD loading.

EXPERIMENTAL PROCEDURES

Polymer synthesis

All polymers used in this study were synthesized by atom transfer radical polymerization, according to literature procedures (26).

Peptide synthesis

The ivDde-protected HIV Tat PTD peptide (sequence: GGYGRK(ivDde)K(ivDde)RRQRRR) was synthesized manually by standard Fmoc solid-phase chemistry. The two ivDde protecting groups for lysine were intentionally left on the peptide prior to and following cleavage from the solid support, using 95% trifluoroacetic acid : 2.5% triisopropylsilane : 2.5% water solution (volume fractions) for 90 minutes. The beads were treated with cleavage solution 3 times total, and the solutions were combined and concentrated *in vacuo*. The concentrate was precipitated into cold ether, and the precipitates were centrifuged at 3500 rpm for 10 min. The supernatant was decanted, the pellet was resuspended in cold ether, and the centrifugation process was repeated. The pellet was purified by reversed phase HPLC. MS (MALDI-ToF): 2087.532 $[M + H]^+$ (calcd: 2087.529).

Spherical micelle formation

Spherical polymer micelles of narrow size distribution were obtained by dissolving the block copolymer PAA_{128}-*b*-PS_{40} (32.5 mg) in DMF (35 mL) followed by gradual addition (4 mL/h) of an equal volume of nonsolvent (H_2O) for the hydrophobic polystyrene to induce micellization. The micelles were stirred for 4 h before being transferred to presoaked and rinsed dialysis bags (MWCO 6−8 kDa) and dialyzed against nanopure water (18.0 MΩ·cm) for 3 days to remove the organic solvent. The final volume was 115 mL of aqueous micelle solution for a final concentration of 0.28 mg/mL. TEM: 11 ± 2 nm (diameter).

Short cylindrical micelle formation

PAA_{96}-*b*-PS_{48} block copolymer (10 mg) was dissolved in THF (50 mL) and was dried in a round-bottom flask *in vacuo*, leaving a thin membrane of the polymer in the flask. To the flask, nanopure water (58.8 mL) was added and then sonicated while rotating in an aqueous sonicator (VMR Aquasonic 75T) for 40 min. The resulting solution contained short cylindrical micelles, which gave a light-blue color to the solution, a characteristic of the light scattering caused by the cylindrical micelle assemblies. The final concentration was 0.17 mg/mL. TEM: 180 ± 120 nm (length) and 20 ± 2 nm (cross-sectional diameter).

Shell-crosslinked spherical and short cylindrical nanoparticle formation

The aqueous solutions of spherical and short cylindrical micellar assemblies of PAA_{128}-*b*-PS_{40} and PAA_{96}-*b*-PS_{48}, respectively, were individually mixed with O-bis-(aminoethyl) ethylene glycol (0.15 equiv., relative to the molar number of available COOH groups) and allowed to stir at room temperature. After 30 min, an aqueous solution of 1-[3'-(dimethylamino)propyl]-3-ethylcarbodiimide hydrochloride (EDCI) (1 equiv., relative to the molar number of available COOH groups) was added. The reaction mixture was allowed to stir overnight before being transferred to presoaked and rinsed dialysis tubing (MWCO 3 kDa) and dialyzed against nanopure water (18.0 MΩ·cm) for 3 days.

Long cylindrical shell-crosslinked nanoparticle formation

To a solution of triblock copolymer PAA_{94}-*b*-PMA_{103}-*b*-PS_{28} (8.4 mg) in THF (8.00 mL) with stirring was added a solution of THF (2.0 mL) containing O-bis-(aminoethyl)ethylene glycol (0.93 mg, 0.15 equiv., relative to COOH groups). The mixture was allowed to stir overnight at room temperature, and then H_2O (40 mL) was added at a rate of 7.50 mL/h to induce micellization. To this water-THF mixture, EDCI (5.6 mg) was added to crosslink the shell domain of the micelle and to lock the morphology (27). The pre-mixing of the diamine crosslinker with the triblock copolymer is essential to the formation of the desired morphology (19). After stirring overnight, the reaction mixture was transferred to presoaked and rinsed dialysis tubing (MWCO 6−8 kDa) and dialyzed against nanopure water (18.0 MΩ·cm) for 3 days to remove the organic solvent. The final volume was 61.3 mL of aqueous crosslinked long, cylindrical micelle solution for a final concentration of 0.14 mg/mL. TEM: 970 ± 900 nm (length) and 30 ± 2 nm (cross-sectional diameter).

Functionalization with fluorescent tag

The respective shell-crosslinked nanoparticle solutions were diluted to the same molar concentration (7.5 μM polymer) and each was placed into a round-bottom flask and cooled to 0 °C using an ice bath. A mixed solution of 1:1, EDCI:N-hydroxysulfosuccinimide (sulfo-NHS) was added to each nanoparticle solution (1.2:1 molar ratio, relative to the available COOH groups) to activate the acrylic acid residues. After 30 minutes, aliquots of Alexa Fluor 594 cadaverine stock solution were added to each flask and the mixtures and were allowed to react overnight. The solutions were then transferred to presoaked dialysis tubing (MWCO 6 −8 kDa) and allowed to dialyze for 5 days against nanopure water.

Functionalization with PTD

Shell-crosslinked nanoparticle solutions pre-functionalized with Alexa Fluor 594 were each placed into a 25 mL round-bottom flask. Sodium chloride was placed into each flask to give a concentration of 5.0 mg/mL, to minimize particle-particle aggregation. The flask was then placed in an ice bath. A mixed solution of 1:1, EDCI:sulfo-NHS was added to each nanoparticle solution (1.2:1 molar ratio, relative to the available COOH groups) to activate the acrylic acid residues. A stock solution (18.21 mg/mL) of the ivDde-protected PTD peptide was made in nanopure water, and aliquots of the solution were added to the respective flasks 30 min after

the addition of EDCI/NHS. The pH of each reaction mixture was adjusted to 7.40 using pH = 8.00 sodium phosphate buffer. The mixtures were allowed to react overnight. The solutions were then transferred to presoaked dialysis tubings (MWCO 12 kDa) and allowed to dialyze for 5 days against nanopure water. At the end of dialysis, the nanoparticle solutions were treated with 2.0% hydrazine for 20 minutes to remove the ivDde protecting groups, and then the pH was adjusted to 6.50 using pH = 6.34 sodium phosphate buffer. The solutions were then transferred to presoaked dialysis tubings (MWCO 100 kDa) for a second-stage dialysis over a period of 15 days. UV-Vis measurements confirmed coupling of the PTD peptide to the shell-crosslinked nanostructures (18). Removal of the ivDde protecting groups under these reaction conditions was confirmed by MALDI-ToF mass spectrometry for a model reaction performed upon non-conjugated PTD peptide (Fig. 3).

Cell Line and Fluorescence Confocal Microscopy

Chinese hamster ovary (CHO) cells (ATCC) were cultured, counted, and resuspended to a final concentration of 100 000 cells/mL. An aliquot of the cell suspension (3.00 mL) was deposited into each well of a tissue culture treated six-well plate (Falcon, 3043), which contained a No. 1.5 glass cover slip (Corning). After 48 h, the cells (50−60% confluence) in each six-well plate were washed with PBS (2 × 5.00 mL). An aliquot of serum free RPMI 1640 media (1.00 mL) was added to each well, followed by the respective nanoparticle solutions (100 μL each). The plates were then returned to the incubator to incubate at 37 °C or 0 °C. Following desired incubation times, the nanoparticles were removed, and each well was washed with Hanks Balanced Salt Solution (HBSS) (3 × 5.00 mL) and viewed under bright field and fluorescent conditions using a Leica TCS SP2 inverted microscope.

Quantitative analysis of confocal images

The background levels of the red channel containing the signal of Alexa Fluor-labeled nanoparticles were determined by the following method: 1. Binary masks corresponding to nanoparticles-associated fluorescence were generated ($Mask_{NP0}$). Threshold levels were determined by visual inspection. 2. $Mask_{NP0}$ was inverted by applying a NOT-operation to generate a binary mask for the background ($Mask_{bg}$). 4. The inverted mask $Mask_{bg}$ was multiplied with the original red channel, Red_0, and the mean value of the resulting image was determined as the background level. Cell fluorescence intensities were determined by the following method: 1. Background noise was subtracted from the original signal, Red_0, giving Red_1. 2. Binary masks were generated ($Mask_{NP1}$) for Red_1. Threshold levels were determined by visual inspection. 3. $Mask_{NP1}$ was multiplied by Red_1. 4. Over the resulting image, individual cells were manually selected as regions of interest (ROI), and mean intensities were recorded for each cell. A minimum of 100 cells was measured for each time point of each sample. The mean intensity values and standard deviation values were calculated.

RESULTS AND DISCUSSION

In order to validate size/shape effects of the nanoparticle carrier in their cell internalization characteristics, mediated by PTD peptide, two series of nanoparticle solutions were prepared. The first series included the same spherical structures with increasing loadings of PTD; the second series contained particles having the same amount of PTD but increasing particle length in one dimension (from 10 nm to several μm). The first series was used to probe the effectiveness of PTD on cell internalization while the second series was used to probe the size/shape effect.

We designed and synthesized shell-crosslinked nanoparticles of different sizes and spherical or cylindrical shapes and then performed further functionalization for fluorescent labeling and PTD attachment to afford the two series of materials (Scheme 1). The spherical nanoparticle

was assembled from a diblock copolymer (poly(acrylic acid)$_{128}$-*b*-polystyrene$_{40}$, PAA_{128}-*b*-PS_{40}). The short and long cylindrical nanoparticles were assembled from a diblock and a triblock copolymer, PAA_{98}-*b*-PS_{48} and poly(acrylic acid)-*b*-poly(methyl acrylate)-*b*-polystyrene (PAA_{94}-*b*-PMA_{103}-*b*-PS_{28}), respectively. All three particles were nominally 30% crosslinked in the shell domain, using standard procedures (28). The spherical particle had an average diameter of 11 ± 2 nm, as evidenced by transmission electron microscopy (TEM). The short cylinder had an average cross-sectional diameter of 20 ± 2 nm, and an average length of 180 ± 120 nm. The long cylinder had an average cross-sectional diameter of 30 ± 2 nm, and an average length of 970 ± 900 nm (Table 1). TEM images (Fig. 1) show the morphologies of the three nanostructures.

Functionalization of the nanostructures with both the fluorescent tag (Alexa Fluor 594 cadaverine) for confocal microscopy and the Tat PTD peptide was achieved by using carbodiimide chemistry. Attachment of the Alexa Fluor 594 to the nanostructures was performed first. To ensure that all final solutions had the same amount of total fluorescence, the solution of spherical particles was then split for further labeling with different amounts of PTD (at levels of 0.5, 1, and 2% consumption of total COOH groups of the PAA_{128}-*b*-PS_{40}), while the solutions of cylindrical nanostructures were functionalized at a level that coincided with the 1% labeling of the spheres. Because the Tat PTD has two lysine residues, whose side chain amine could compete with the terminal amine for the activated carboxylic acid on the nanoparticle, ivDde protecting groups were used to cap the lysine residues and were subsequently removed, after the Tat PTD was coupled to the nanoparticle (Scheme 2). A model study on aqueous ivDde removal by Matrix-Assisted Laser Desorption Ionization-Time of Flight (MALDI-ToF) mass spectrometry demonstrated adequate removal under reaction with 2% hydrazine in water (Fig. 3). These reaction conditions were fairly mild to the nanoparticle framework, although some amount of the AlexaFluor 594 cadaverine was cleaved. Therefore, all samples, even the control particles without PTD were treated to these deprotection reaction conditions. Extensive dialysis was used to remove unbound peptide, which previously has been reported to be effective (18). Both the fluorescent dye and the Tat PTD were loaded successfully within the nanoparticles, as evidenced by UV-Vis spectroscopy (Fig. 4), although it is not clear whether all detected peptide was covalently bound or electrostatically adsorbed onto or absorbed into the nanoparticles, due to their oppositely and highly positively-charged characteristics. For the cylindrical particles, accurate UV-Vis measurement was complicated by light scattering and, therefore, the assumption was made that the coupling yields for all particles were similar (Fig. 5). After functionalization, the morphologies of each nanostructure did not undergo discernible changes, as confirmed by TEM (images not shown).

Because the PTD peptides were conjugated after the micellization and crosslinking and should be present on the particles' surfaces, the surface areas of the nanostructures determine the number of peptides loaded onto each particle given the total amount of PTD peptide, assuming the particles' densities are similar (29). The three nanostructures each represented a unique size distribution, with the greatest percentage surface area for each morphology being separated by an order of magnitude (Fig. 1).

To verify the effectiveness of CPP, spherical particles of the same size loaded with different amounts of CPP (series 1) were incubated with CHO cells at a concentration of 0.68 μM (polymer) at 37 °C and 0 °C for 1 hour. Confocal microscopy imaging of non-fixed, live cells suggests that CPP had a pronounced enhancement in the uptake of the nanoparticles by the CHO cells (Fig. 6). The highest amount of PTD loading, 2.0%, gave nanoparticles that exhibited nearly a 5-fold increase in cell uptake at 37 °C, than the nanoparticles without PTD. Incubation at 0 °C, under otherwise the same conditions, resulted in little cell uptake. The difference in cell uptake at different temperatures can be due to reduced membrane permeability at low temperatures, to the energy-dependency of the uptake process, or to both.

An interesting phenomenon we noticed is that the PTD-nanoparticle conjugates were both contained within cellular vesicles and partly spread into the cytoplasm, with exclusion from the nucleus, whereas PTD alone has been reported to accumulate selectively in the cell nucleus (31,32). This observation is possibly due to the overall negatively-charged nature of the PTD-particle conjugate or may be due to comparisons between different cell lines.

To probe the size/shape effect, we loaded the three differently-shaped particles with a fixed amount of PTD (equivalent to 1% of the carboxylates of PAA_{128}-*b*-PS_{40}), and incubated CHO cells in their solutions under the same buffer condition as above at 37 °C for 1 hour. It was found that the smaller, spherical particle had higher cell uptake than the larger, cylindrical nanoparticles (Fig. 7). Based on these results, we can speculate on the general mechanisms that govern the transduction of the PTD-functionalized nanomaterials. Many variables determine the uptake rate, including adhesion rate and receptor diffusion kinetics. Freund *et al* (33) and Bao *et al* (34) have modeled these factors and developed a hypothesis involving "wrapping time" of the membrane; the shorter the wrapping time, the faster is the uptake. It has been predicted theoretically by this model that through the competition between thermodynamic driving force and diffusion kinetics, there is an optimum radius for efficient "wrapping", which is 27−30 nm. Because the early endocytic vesicles are usually less than 100 nm in diameter (6), most short cylindrical particles (average length = 170 nm) would have to be curved or bent to be internalized, which requires additional energy. Therefore, although the cylindrical particles have higher surface area and hence more membrane-particle interaction (less diffusion), the system is not able to either overcome the overall lack of thermodynamic driving force caused by having to bend the cylinders to "fit" in the endosomes or to create larger endocytic vesicles to contain the cylindrical nanostructures. Another factor, for the higher uptake of the small, spherical particle by the cell at a given time, is the higher particle molar concentration for the spheres, which is the result of the lower aggregation number for the spherical particle, compared with the cylindrical particle. For example, the average short cylinder occupies *ca.* 80 times as much volume as does the sphere, based on calculations from TEM cross-sectional and longitudinal measurements.

Last, we investigated the release of the PTD-nanoparticle conjugates from CHO cells. CHO cells were incubated with 0.68 μM particle solutions for 1 h at 37 °C. Following the incubation period, the nanoparticle-containing solutions were removed, the cells were washed with PBS, and serum free RPMI 1640 media was introduced, followed by further incubation. Fluorescence monitoring of CHO cells immediately after buffer change, and at 2, 4 and 8 h time points revealed that fluorescence intensity decreased over time for spherical nanoparticles labeled with 2%, 1% and 0.5% PTD, suggesting particles being released from the cell (Fig. 8). The rates of release of spherical particles appeared to be dependent on the amount of PTD loaded on the nanoparticle, for which the highest loading (2%) led to the fastest release. This result could suggest that PTD-assisted particle transduction works in a two-way fashion: both entry and exit seem to be facilitated by PTD (35). The cells that had been incubated with spheres having no PTD did not show apparent decrease of fluorescence over 8 h. Both the long and short cylinders behaved similarly as the spheres without the PTD peptide, showing little uptake and no measurable release. Other PTD-independent processes, such as peptide degradation are possible, and thus more detailed studies on cell uptake and release of differently-shaped nanostructures are needed to reveal a fuller picture of the mechanisms involved.

CONCLUSIONS

The self assembly of block copolymers afforded spherical nanostructures and cylindrical nanostructures having distinctive lengths required to investigate the effects of different particle sizes and shapes, across a wide size range (10 nm - 1000 nm), upon cell transduction. Attachment of the Tat cell penetration peptide of HIV-1 improved cell internalization of the

spheres. The amount of cell uptake was a function of PTD loading, with increasing amounts of PTD providing for increasing levels of cell internalization at a given time point. Attachment of PTD to the small cylinders (~200 nm) and long cylinders (~ 1000 nm) did not produce detectable increase in cell uptake. Once internalized, the PTD-spherical nanoparticle conjugates escaped from the cell at a rate that was a function of PTD loading. The observation of reversible cell transduction will become important as these nanostructures are functionalized also with ligands that are designed to probe intracellular targets, so that escape from cells lacking the target can be facilitated to allow for the nanostructures to accumulate in the designated cells.

The polymer micelle-based nanoparticles in this study have enabled comparison of size and shape on cellular uptake, for materials that have the same surface chemistry, differing only in their core composition, size and shape. Further studies are required to understand fully the mechanisms by which the particle characteristics lead to the observed differences in cellular uptake and release. Moreover, the particles and the methodologies for functionalization described herein can be employed for fundamental studies that extend to systems involving ligand-receptor interactions to promote endocytosis, which will be important to gain new insights into the interface of biological systems with synthetic nanostructures. These results also serve as a guideline in engineering artificial nanoscale carrier particles for drug delivery, where the control of size/shape is of significance.

ACKNOWLEDGMENT

The authors gratefully acknowledge support from the National Heart Lung and Blood Institute of the National Institutes of Health as a Program of Excellence in Nanotechnology (NHLBI-PEN HL080729). The authors also thank senior microscopist G. Michael Veith of the Washington University Department of Biology Microscopy Facility for providing technical support with TEM and fluorescence confocal microscopy.

LITERATURE CITED

1. Duchardt F, Fotin-Mleczek M, Schwarz H, Fischer R, Brock R. A comprehensive model for the cellular uptake of cationic cell-penetrating peptides. Traffic 2007;8:848–866. [PubMed: 17587406]
2. Chithrani BD, Chan WCW. Elucidating the mechanism of cellular uptake and removal of protein-coated gold nanoparticles of different sizes and shapes. Nano Lett 2007;7:1542–1550. [PubMed: 17465586]
3. Hyunmin K, Robert D, H FM, L JR. Tat-conjugated PAMAM dendrimers as delivery agents for antisense and siRNA oligonucleotides. Pharm Res 2005;22:2099–20106. [PubMed: 16184444]
4. Matthaeus C, Kale A, Chernenko T, Torchilin V, Diem M. New ways of imaging uptake and intracellular fate of liposomal drug carrier systems inside individual cells, based on Raman microscopy. Mol Pharmaceutics ASAP. 2008
5. Kam NWS, Dai H. Carbon nanotubes as intracellular protein transporters: Generality and biological funcitonality. J Am Chem Soc 2005;127:6021–6026. [PubMed: 15839702]
6. Osaki F, Kannamori T, Sando S, Sera T, Aoyama Y. A quantum dot conjugated sugar ball and its cellular uptake. On the size effects of endocytosis in the subviral region. J Am Chem Soc 2004;126:6520–6521. [PubMed: 15161257]
7. Foerg C, Merkle HP. On the biomedical promise of cell penetrating peptides: limits *versus* prospects. J Pharm Sci 2007;97:144–162. [PubMed: 17763452]
8. Chithrani BD, Chazani AA, Chan WCW. Determining the size and shape dependence of gold nanoparticle uptake into mammalian cells. Nano Lett 2006;6:662–668. [PubMed: 16608261]
9. Champion JA, Mitragotri S. Role of target geometry in phargocytosis. Proc Natl Acad Sci USA 2006;103:4930–4934. [PubMed: 16549762]
10. Geng Y, Dalhaimer P, Cai S, Tsai R, Tewari M, Miniko T, Discher DE. Shape effects of filaments *versus* spherical particles in flow and drug delivery. Nature Nanotech 2007;2:249–255.

11. Read ES, Armes SP. Recent advances in shell cross-linked micelles. Chem Commun 2007:3021–3035.
12. Krikorian, V.; Kang, Y.; Thomas, EL. Self-assembly and morphology diagrams for solution and bulk materials: Experimental aspects. In: Matyjaszewski, K.; Gnanou, Y.; Leibler, L., editors. Macromolecular Engineering. Wiley-VCH Verlag GmbH & Co. KGaA; Weinheim, Germany: 2007. p. 1387-1430.
13. Hamley I. Nanoshells and nanotubes from block copolymers. Soft Matter 2005;1:36–43.
14. Sun GX, J. Hagooly A, Rossin R, Li Z, Moore DA, Hawker CJ, Welch MJ, Wooley KL. Strategies for optimized radiolabeling of nanoparticles for *in vivo* PET imaging. Adv Mater ASAP. 2007
15. Rossin R, Pan D, Qi K, Turner JL, Sun X, Wooley KL, Welch MJ. ^{64}Cu-labeled folate-conjugated shell cross-linked nanoparticles for tumor imaging and radiotherapy: Synthesis, radiolabeling, and biologic evaluation. J Nucl Med 2005;46:1210–1218. [PubMed: 16000291]
16. Yang T-F, Chen C-N, Chen M-C, Lai C-H, Liang H-F, Sung H-W. Shell-crosslinked Pluronic L121 micelles as a drug delivery vehicle. Biomaterials 2006;28:725–734. [PubMed: 17055046]
17. Lazzari, M.; Liu, G.; Lecommandoux, S. Block Copolymers in Nanoscience. Wiley-VCH Verlag GmbH & Co. KGaA; Weinheim, Germany: 2006.
18. Becker ML, Remsen EE, Pan D, Wooley KL. Peptide-derivatized shell-cross-linked nanoparticles. 1. Synthesis and characterization. Bioconjugate Chem 2004;15:699–709.
19. Cui H, Chen Z, Wooley KL, Pochan DJ. Controlling micellar structure of amphiphilic charged triblock copolymers in dilute solution *via* coassembly with organic counterions of different spacer lengths. Macromolecules 2006;39:6599–6607.
20. Cui H, Chen Z, Zhong S, Wooley KL, Pochan DJ. Block copolymer assembly *via* kinetic control. Science 2007;317:647–650. [PubMed: 17673657]
21. Discher DE, Eisenberg A. Polymer vesicles. Science 2002;297:967–973. [PubMed: 12169723]
22. Pressly ED, Rossin R, Hagooly A, Fukukawa K-I, Messmore BW, Welch MJ, Wooley KL, Lamm MS, Hule RA, Pochan DJ, Hawker CJ. Structural effects on the biodistribution and positron emission tomography (PET) imaging of well-defined (64)Cu-labeled nanoparticles comprised of amphiphilic block graft copolymers. Biomacromolecules 2007;8:3126–3134. [PubMed: 17880180]
23. Pochan DJ, Chen Z, Cui H, Hales K, Qi K, Wooley KL. Toroidal triblock copolymer assemblies. Science 2004;306:94–97. [PubMed: 15459386]
24. Turner JL, Pan D, Plummer R, Chen Z, Whittaker AK, Wooley KL. Synthesis of gadolinium-labeled shell-crosslinked nanoparticles for magnetic resonance imaging applications. Adv Funct Mater 2005;15:1248–1254.
25. Pan D, Turner JL, Wooley KL. Shell cross-linked nanoparticles designed to target angiogenic blood vessels *via* $\alpha_V\beta_3$ receptor-ligand interactions. Macromolecules 2004;37:7109–7115.
26. Ma Q, Wooley KL. The preparation of tbutyl acrylate, methyl acrylate, and styrene block copolymers by atom transfer radical polymerization: precursors to amphiphilic and hydrophilic block copolymers and conversion to complex nanostructured materials. J Polym Sci Part A: Polym Chem 2000;38:4805–4820.
27. Ma Q, Remsen EE, Christopher G, Clark J, Kowalewski T, Wooley KL. Chemically induced supramolecular reorganization of triblock copolymer assemblies: trapping of intermediate states *via* a shellcrosslinking methodology. Proc Natl Acad Sci USA 2002;99:5058–5063. [PubMed: 11929963]
28. Huang H, Remsen EE, Wooley KL. Amphiphilic core-shell nanospheres obtained by intramicellar shell crosslinking of polymer micelles with poly(ethylene oxide) linkers. Chem Commun 1998:1415–1416.
29. Remsen EE, K. Bruce Thurmond I, Wooley KL. Solution and surface charge properties of shell-crosslinked knedel nanoparticles. Macromolecules 1999;32:3685–3689.
30. Kam NWS, Liu Z, Dai H. Carbon nanotubes as intracellular transporters for proteins and DNA: An investigation of the uptake mechanism and pathway. Angew Chem Int Ed 2006;45:577–581.
31. Ziegler A, Nervi P, Durrenberger M, Seelig J. The cationic cell-penetrating peptide CPP(TAT) derived from the HIV-1 protein TAT is rapidly transported into living fibroblasts: Optical, biophysical, and metabolic evidence. Biochemistry 2005;44:138–148. [PubMed: 15628854]

32. Ziegler A, Seelig J. High affinity of the cell-penetrating peptide HIV-1 Tat-PTD for DNA. Biochemistry 2007;46:8138–8145. [PubMed: 17555330]

33. Gao H, Shi W, Freund LB. Mechanics of receptor-mediated endocytosis. Proc Natl Acad Sci USA 2005;102:9469–9474. [PubMed: 15972807]

34. Bao G, Bao XR. Shedding light on the dynamics of endocytosis and viral budding. Proc Natl Acad Sci USA 2005;102:9997–9998. [PubMed: 16009932]

35. Hirano K, Hirano M, Nishimura J, Kanaide H. A critical period requiring Rho proteins for cell cycle progression uncovered by reversible protein transduction in endothelial cells. FEBS Letters 2004;570:149–154. [PubMed: 15251456]

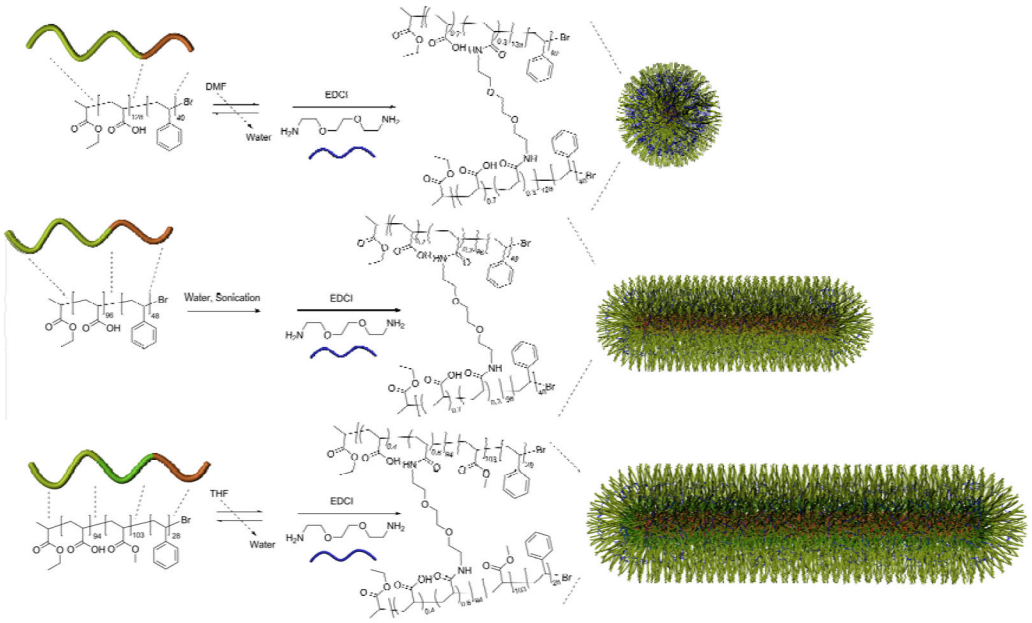

Scheme 1.

Block copolymers (PAA_{128}-*b*-PS_{40}, PAA_{98}-*b*-PS_{48} and PAA_{94}-*b*-PMA_{103}-*b*-PS_{28}) were micellized by different procedures, to afford spherical and cylindrical nanoparticles of different cross-sectional diameters and lengths.

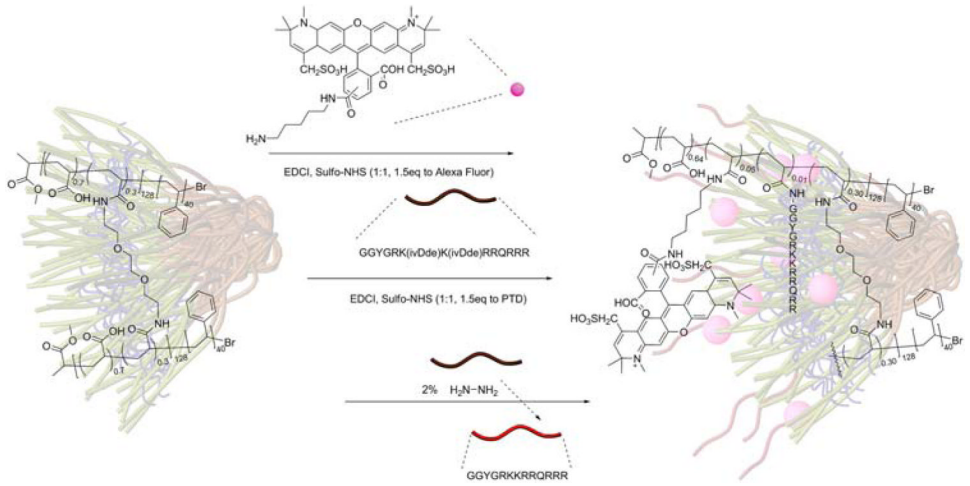

Scheme 2.

Functionalization of the spherical nanoparticle sample was achieved through a three-step synthesis. Alexa Fluor 591 and protected PTD were respectively coupled to the nanoparticle *via* carbodiimide chemistry. The ivDde protecting groups were removed by treatment with a 2.0% hydrazine solution in water.

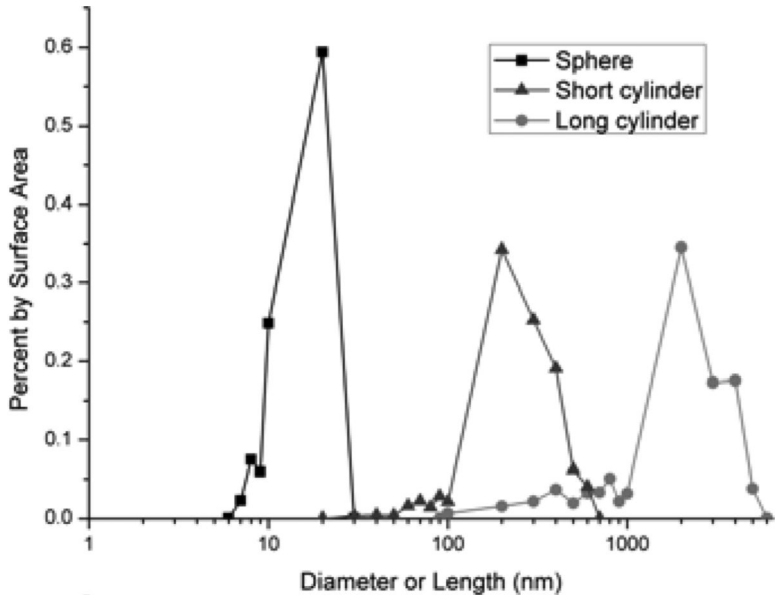

Figure 1.
Size distribution by surface area. The size of the three nanostructures is each separated by an order of magnitude.

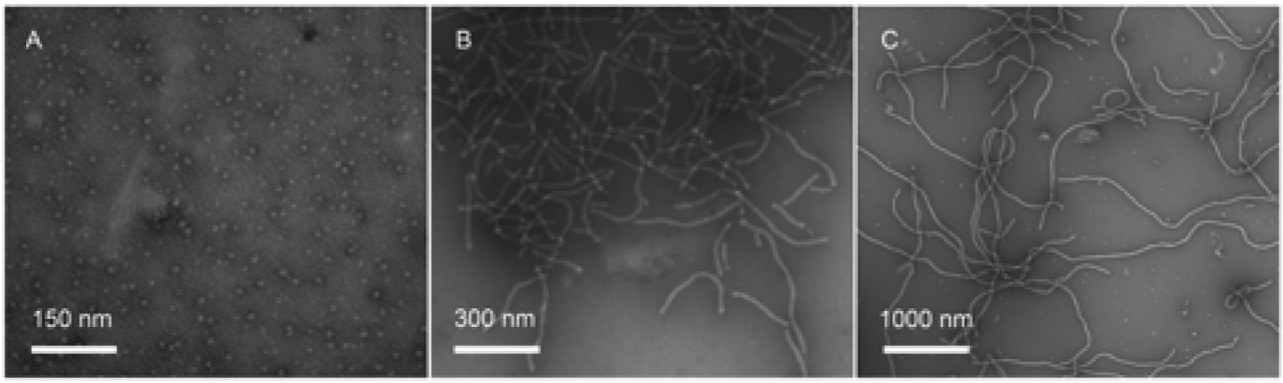

Figure 2.
TEM of PAA_{128}-*b*-PS_{40} (A), PAA_{98}-*b*-PS_{48} (B) and PAA_{94}-*b*-PMA_{103}-*b*-PS_{28} (C) micelles in nanopure water.

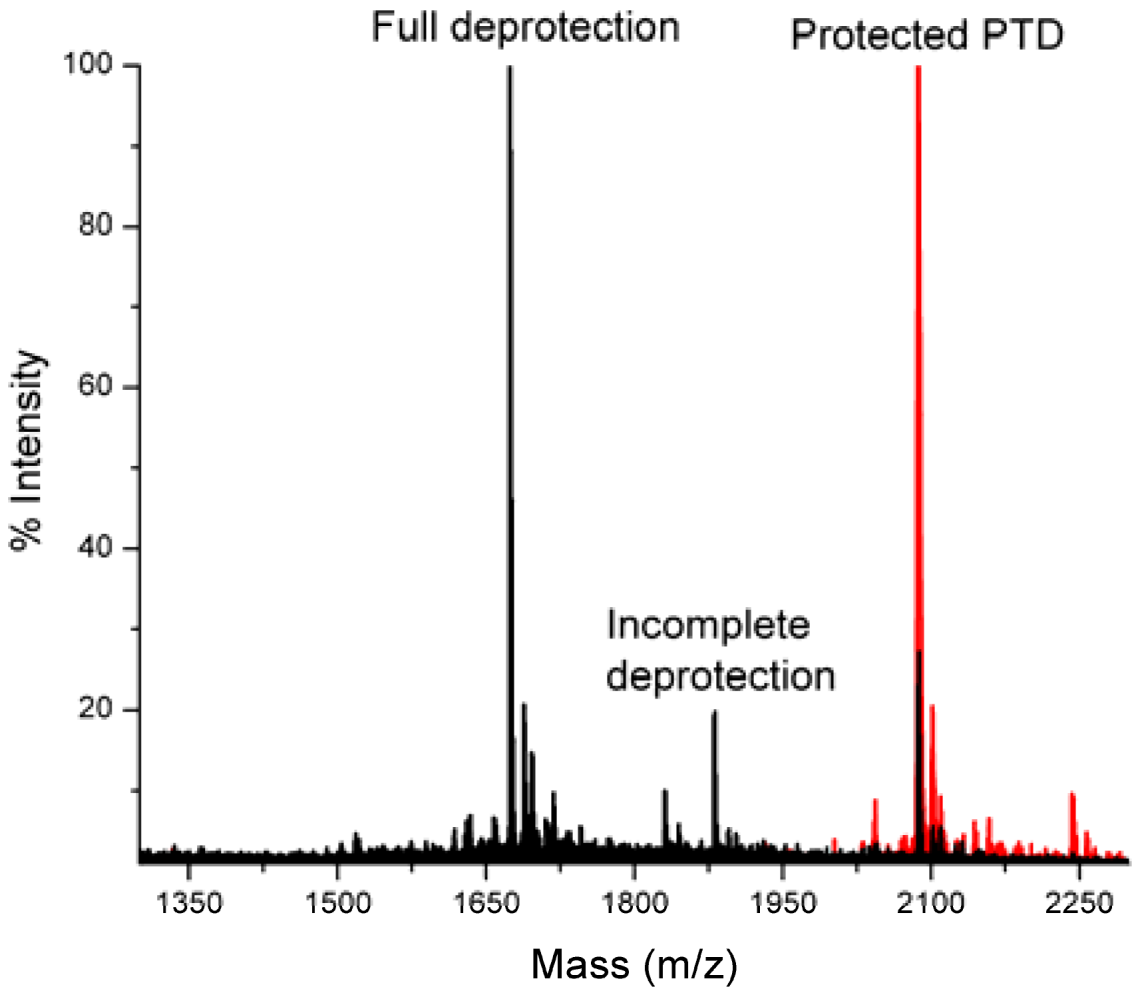

Figure 3.
Overlaid MALDI-ToF spectra of ivDde-protected PTD before and after treatment with 2.0% hydrazine for 20 minutes in water. Adequate removal of ivDde (>70%) was achieved, despite the deprotection reaction being less efficient in water than in organic solvent.

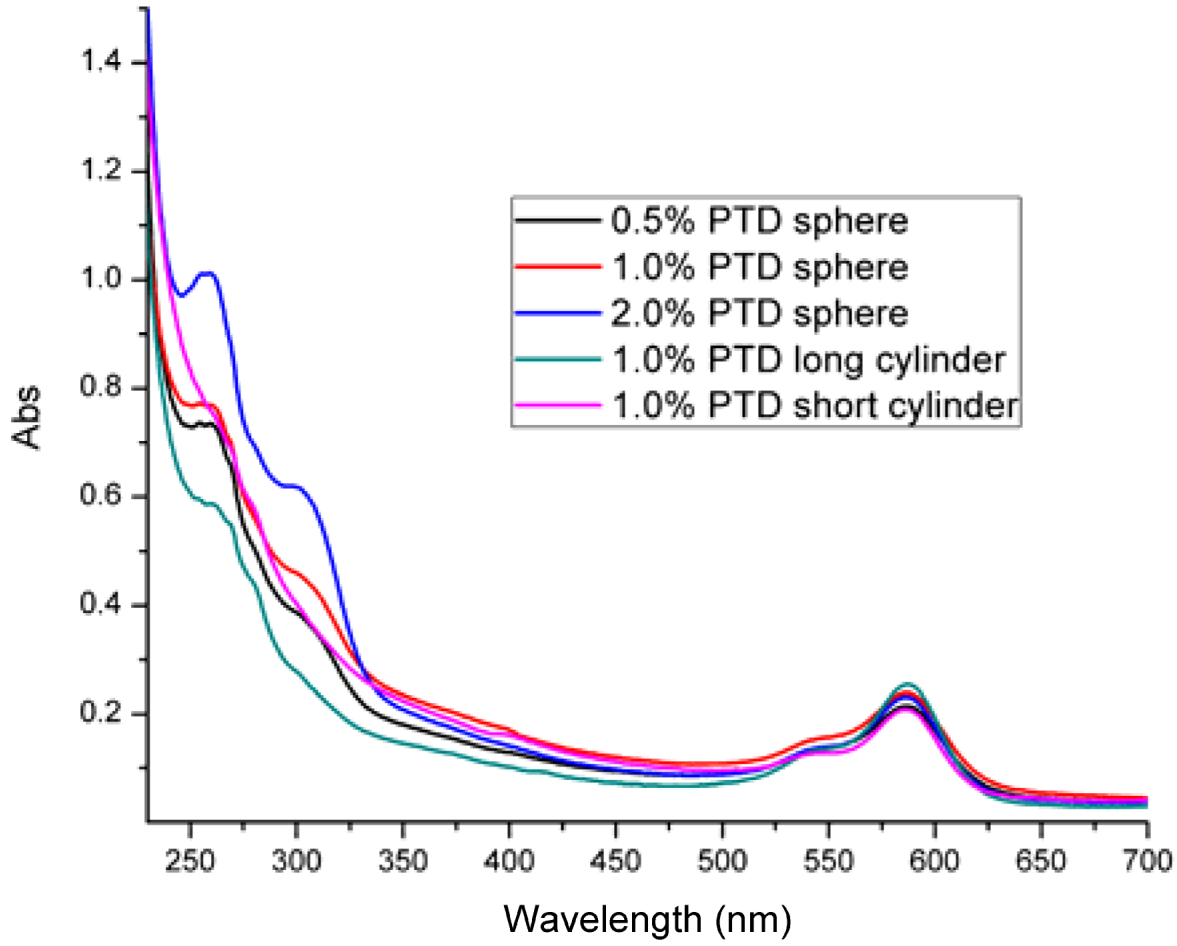

Figure 4.
UV-Vis spectra of spheres and cylinders labeled with Alexa Fluor 594 cadaverine and PTD peptide.

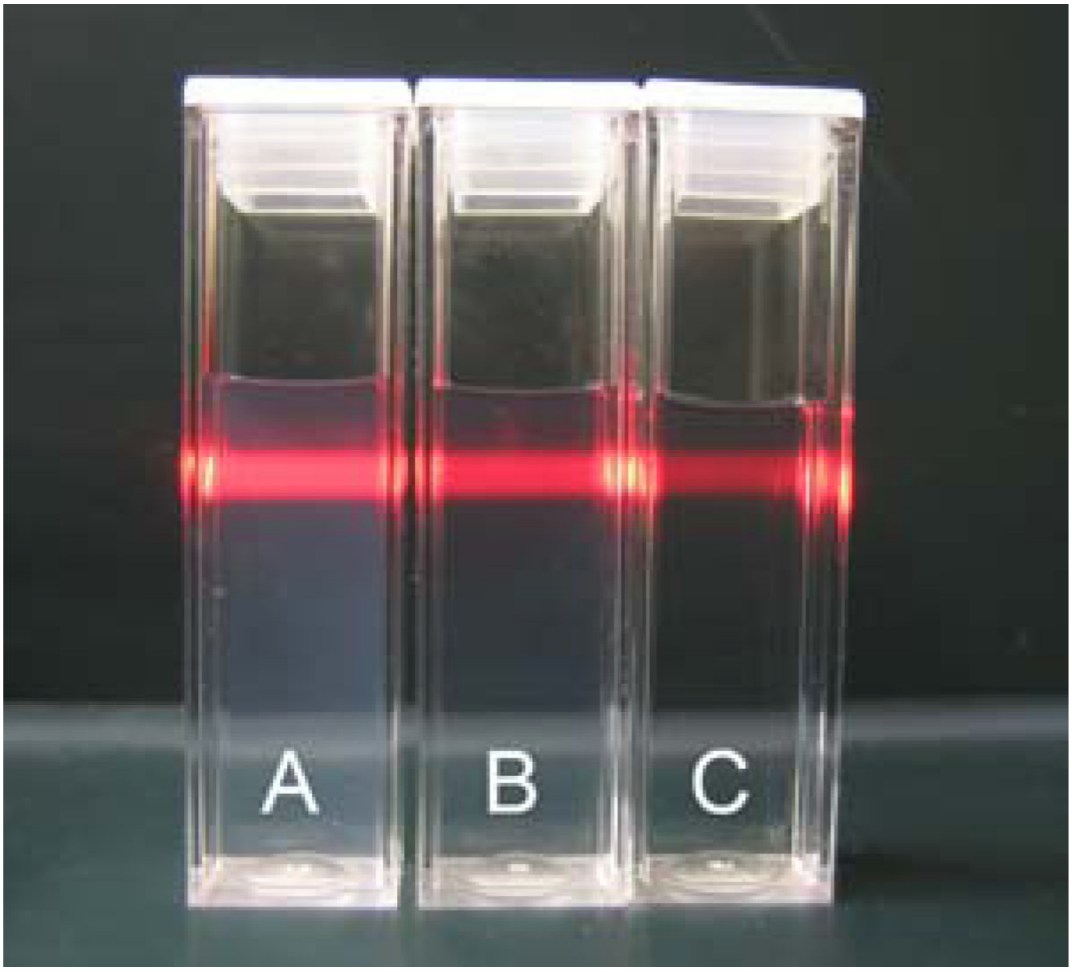

Figure 5.
Light scattering of the long cylinders complicates accurate UV-Vis measurement. A: Long cylinders. B: Short cylinders. C: Spheres.

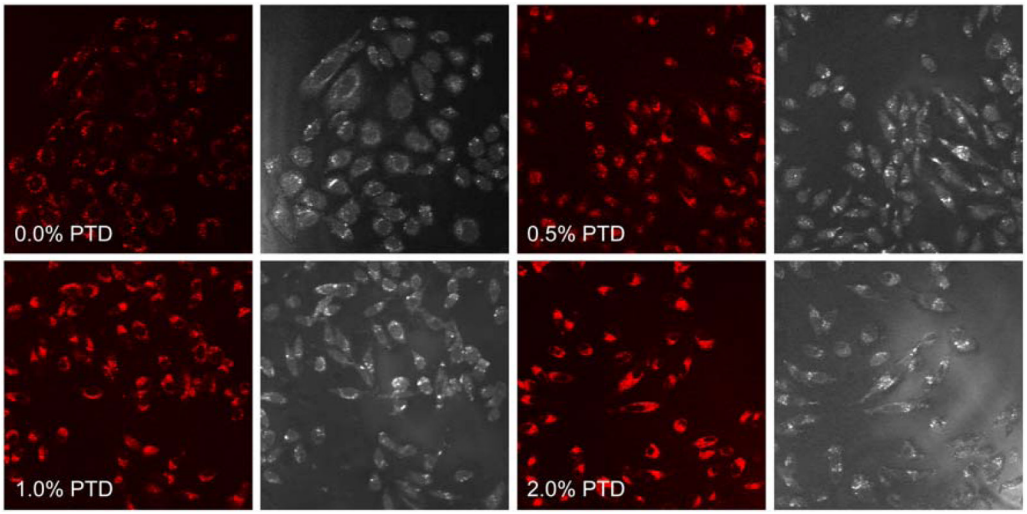

Figure 6.
Confocal images of CHO cells incubated with the spherical nanoparticles having different amounts of PTD for 1 hour. Cell uptake of PTD-sphere conjugates increased by the action of increasing loadings of surface-bound PTD peptide.

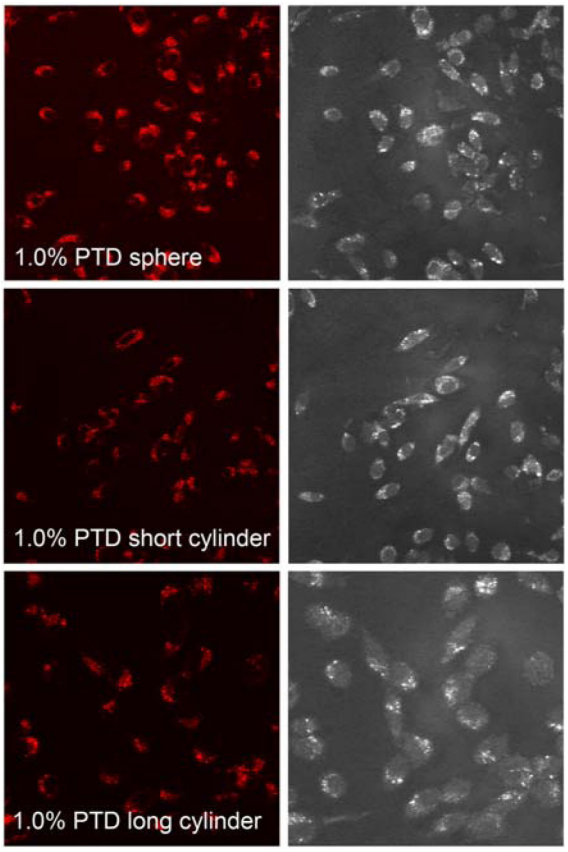

Figure 7.
When conjugated with the same amount of PTD peptide, greater amounts of the smaller, spherical nanoparticles were internalized than were the larger, cylindrical nanoparticles. Images were taken after 1 hour of incubation.

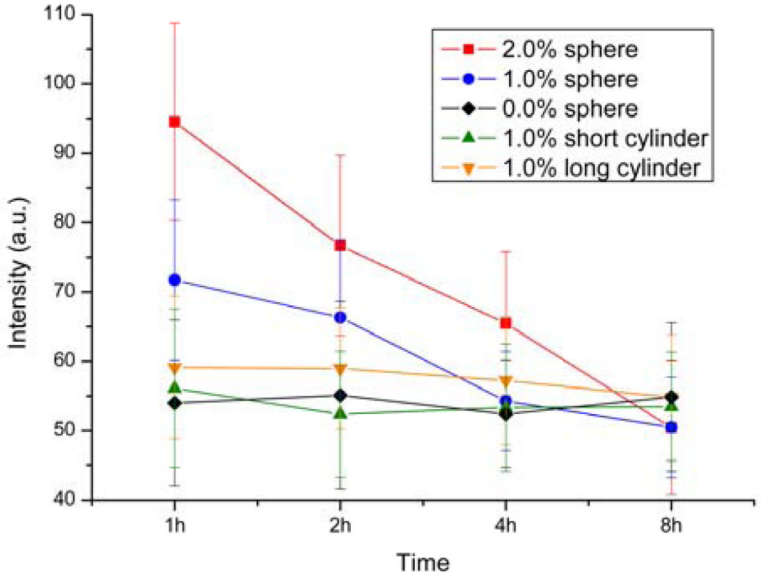

Figure 8.
Release profile of series 1 nanoparticles (spherical in shape; different amounts of PTD peptide) and series 2 nanoparticles (different shapes; each with 1.0% PTD peptide conjugation).

Table 1

Dimensions of the nanostructures evaluated.

Sample	Cross-sectional diameter (nm)	Length (nm)
Sphere	11 ± 2	n. a.
Short Cylinder	20 ± 2	180 ± 120
Long Cylinder	30 ± 2	970 ± 900